Transaction B: Mechanical Engineering
Vol. 17, No. 4, pp. 264–284

SCIENTIA IRANICA

Classification of Mean Arterial Pressure Regimes in ICU Using a Model-Based Support Vector Machine: Acute Hypotensive, Critical and Survival Episodes

A. Ghaffari[1,2], M.R. Homaeinezhad[1,2,*], M. Akraminia[1,2], M. Atarod[2,3] and R. Rahmani[4]

Abstract. *In this study, a new pattern discrimination method for the classification of Mean Arterial Pressure (MAP) regimes in ICU via an appropriately regulated Radial Basis Function (RBF) Support Vector Machine (SVM) is described. The aim of this classification is to detect hazardous cardiogenic shock situations to prevent probable fatal failure of organs. To this end, first, electrocardiogram (ECG) and Blood Pressure (BP) waveforms are processed via a Modified Hilbert Transform (MHT), and QRS complexes (equivalently obtaining heart rate-HR trend) and pressure pulses (equivalently obtaining trends of systolic, diastolic and mean arterial pressures) are detected, respectively. In the next step, a RBF-SVM classifier is tuned using features obtained from the cardiogenic shock risk scoring model developed by Hasdai et al. (2000) to classify MAP regimes into three categories; survival (the status that will not fall into shock), critical (the transient status that may lead to shock or a return to the survival episode) and Acute Hypotensive Episode -AHE (meaning cardiogenic shock will certainly occur.) Then, the regulated RBF-SVM classifier is applied to 60 records of the Computers in Cardiology (CinC) Challenge 2009 and the values of Se = 92% and P+ = 93% are obtained for sensitivity and positive predictivity, respectively. As some results of this study, the proposed classification method recognized truly 15 subjects out of 15 normal (without shock episodes) subjects of the MIMICII database as belonging to the "survival class", while the algorithm could classify 24 subjects as "AHE", 3 subjects as of the "critical class" and 3 subjects as in the "survival" situation out of 30 shock containing records of the MIMICII database.*

Keywords: *Acute hypotensive episode; Cardiogenic shock; Blood pressure pulse detection; Piecewise polynomial fitting; Support vector machine; Risk scoring model.*

INTRODUCTION

AHE is one of the most critical events that occur in Intensive Care Units (ICUs) and requires effective and prompt intervention. It is generally defined as any period of 30 minutes or more during which at least 90% of the MAP measurements are at or below 60 mmHg [1]. AHE can lead to intense organ damage and death if not treated appropriately. Diagnosing the causes of this episode including sepsis, myocardial infarction, cardiac arrhythmia, pulmonary embolism, hemorrhage, dehydration, hypovolemia, insufficient cardiac output, or vasodilatory shock, and conducting timely and proper intervention can remarkably reduce the risk of this fatal episode [2-4].

In this context, Cowley et al. [5] investigated the role of the baroreceptor reflex in the daily control of Arterial Blood Pressure (ABP) and concluded that the hypotension in denervated dogs was proportional to the preexisting arterial blood pressure level. Hasdai et al. [6] analyzed baseline variables associated with the development of shock after thrombolytic therapy and devised a scoring system predicting the risk of shock. An innovative study was then conducted by Picard et al. [7] to identify the echocardiographic features of cardiogenic shock, and assess the advantages of

1. *Department of Mechanical Engineering, K.N. Toosi University of Technology, Tehran, P.O. Box 19395-1999, Iran.*
2. *Cardiovascular Research Group (CVRG), K.N. Toosi University of Technology, Tehran, Iran.*
3. *School of Biomedical Engineering, University of Calgary, Alberta, Canada.*
4. *Cardiovascular Division of Imam Khomeini Hospital, Tehran University of Medical Science (TUMS), Tehran, Iran.*
*. *Corresponding author. E-mail:mrezahomaei@dena.kntu.ac.ir*

Received 23 May 2009; received in revised form 28 December 2009; accepted 1 June 2010

the findings on early echocardiograms associated with mortality after cardiogenic shock. Afterwards, Morris et al. [8] proposed a potential algorithm for hypotension based on reports of hypotension during anesthesia from the first 4000 incidents reported to the Australian Incident Monitoring Study (AIMS). An ECG-based method was next developed by Solem et al. [9] for the detection of acute hypotension, which was able to provide information regarding the patient's propensity to hypotension at an early stage of hemodialysis. In another study conducted by Halkin et al. [10], seven risk factors were identified as accurate predictors of mortality for cardiogenic shock. According to their research, measurement of the baseline left ventricular function was the single most powerful predictor of survival, which should be incorporated into risk score models. Recently, multivariable logistic regression modeling techniques are used by Zhang et al. [11] to develop a model for predicting the occurrence of cardiogenic shock. On the basis of the coefficients in their model, they developed a risk score for the probability of cardiogenic shock. This year, the subject of Computers in Cardiology (CinC) Challenge 2009 was about the detection and prediction of AHE phenomenon from some selected records of the MIMICII database [12]. In the original work of Chen et al. [13], six indices are introduced to predict AHE phenomenon: the 5-minute average of MAP vital signs before the forecast window, the 5-minute average of the ABP waveform before the forecast window, the optimal exponentially weighted average of the 10-hour ABP mean before the forecast window, the ABP mean value at the midpoint of the forecast window via linear regression of the 1-hour ABP mean trend before the forecast window, the five minute average of the diastolic vital sign before the forecast window, and a combined index consisting of the 5-minute averages of the second and fifth indices. Herriques and Rocha [14] introduced a generalized regression neural network multi model, which is introduced for the prediction of AHE. Multi model schemes do not recursively use model outputs as inputs for the step ahead of prediction. Therefore, prediction errors are not propagated over the forecast horizon and long term predictions can accurately be estimated. In the study of Langley et al. [15], an automated computer prediction algorithm is introduced in which an AHE index was based on the observation that patients with documented AHE experienced more transient reductions in MAP compared to those without AHE. Mneimneh and Povinelli [16] proposed three approaches that were used to determine a method for the prediction of AHE. Their classification approach is based on a reconstructed phase space neural network approach, K-nearest neighborhood, and a rule based methodology. In the work of Chiarugi et al. [17], significant features are extracted from ABP and HR time series and a median filter is used to suppress most artifacts. A decision tree classification is then designed based on the obtained features and is compared with SVM classification. Fournier and Roy [18] proposed a method in which the ABP trend is used for feature extraction and the Kullback-Liebler divergence between to identify the most discriminative features. In this algorithm, the nearest neighborhood method is used as the classification routine. In the model of Hayn et al. [19], a system including several standard algorithms, most of them for ECG processing, as well as diverse algorithms designed for specific purposes and applications, is introduced. Jin and Stockbridge [20] proposed cubic b-splines used to approximate MAP curves. b-splines generally reflect the local features of the target curve and a rank-based discrimination algorithm is used as the classification scheme. In the work of Jousset et al. [21], the MAP trend is used as the source of the feature selection and a SVM classifier is implemented to categorize the MAP modes into two AHE and normal subgroups. In the model of Ho and Chen [22], after the calculation and processing of the MAP trend in a 30 minute long window frame, the obtained segments are allocated into some bins to form a histogram for the analysis; using color histograms is a very well known method in computer vision and pattern recognition. The presented study concentrates on the detection of AHE and MAPDRs on the basis of the ECG signal and ABP waveform measurements. To this end, the QRS complexes and end-systolic end-diastolic pulses are first identified using two versions of the MHT algorithm, namely ECGMHT and BPMHT, respectively. Then, using the obtained SBP and DBP waveforms, the MAP trend is specified. Afterwards, in order to smooth the fast fluctuations observed in the RR-tachogram and MAP trend, we have designed an innovative smoothing algorithm based on Piecewise Polynomial Fitting (PPF) (see Figure 1). Fitting N numbers of polynomials sequentially to the original signal and determining the corresponding coefficients based on the BLUE approach [23], is the basis of the PPF algorithm operation. In order to consider the mutual influence of parameters on the evaluation of shock probability, a RBF-SVM classifier is regulated using Hasdai et al. parameters as input, with appropriate exponential kernel functions for each parameter. Using this network, it will be possible to incorporate the possible mutual influences between risk parameters, such as Heart Rate (HR), Systolic Blood Pressure (SBP), Diastolic Blood Pressure (DBP), age, gender, weight and some miscellaneous factors, to the calculation of shock occurrence probability. The block diagram of the present study is illustrated in Figure 1. Finally, the proposed algorithm is applied to 60 subjects of the MIMICII Database, and AHE and MAPDRs are consequently detected (MAP $\leq$

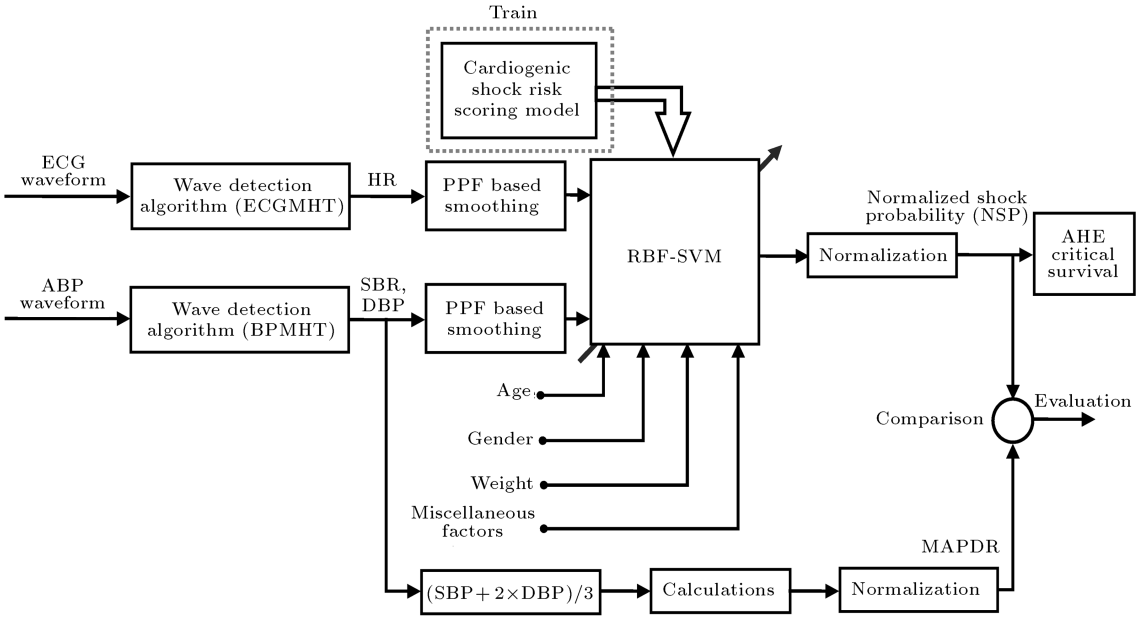

Figure 1. General overview of the proposed shock probability evaluation algorithm via a RBF-SVM trained model.

60 mmHg with endurance more than 30 minutes). The regulated RBF-SVM classifier is applied to 60 records of the MIMICII and the values of Se = 92% and $P+ = 93\%$ are obtained for sensitivity and positive predictivity, respectively. As some results of this study, the proposed classification method recognized truly 15 subjects out of 15 normal (without shock episodes) subjects of the MIMICII database as belonging to the "survival class", while the algorithm could classify 24 subjects as "AHE", 3 subjects as belonging to the "critical class" and 3 subjects as being in a "survival" situation out of 30 shock containing records of the MIMICII database.

MATERIALS AND METHODS

Modified Hilbert Transform (MHT) Algorithm

Conventional Hilbert Transform for Local Extremum Detection

A quadrature filter with the following transfer function is called a Hilbert transform, which is an all-pass filter that changes the phase of the input signal $-90°$ and has an impulse response of $1/(\pi t)$ [24]:

$$G(\omega) = -j\text{sign}(\omega) = \begin{cases} -j & \omega > 0 \\ 0 & \omega = 0 \\ +j & \omega < 0 \end{cases} \quad (1)$$

Therefore, the Hilbert transform of the signal $s(t)$ can be obtained from the following convolution:

$$s_H(t) = s(t) * \frac{1}{\pi t} = \frac{1}{\pi}\int_{-\infty}^{+\infty} \frac{s(\lambda)}{t-\lambda} d\lambda. \quad (2)$$

The most significant characteristic of the Hilbert transform is its mapping of local maxima and minima values of the original signal to the values crossing the zero [24,25]. Assume that $y(t)$ represents the original ECG signal and;

$$y_0(t) = y(t) * h_{\text{BP}}(t), \quad (3)$$

where $h_{\text{BP}}(t)$ is the impulse response of the bandpass FIR filter, and $y_0(t)$ is the output of the filter. Suppose:

$$y_1(t) = \text{Hilbert}[y_0(t)],$$

$$t = 0, 1, 2, \cdots, n_t - 1. \quad (4)$$

Also, assume that the signal $y(t)$ represents an ECG lead, in which R-peaks are upward. As seen in Figure 2 (sections a to g), a sign change from positive to negative in the Hilbert transform of a signal is an indicator of the existence of a local maximum; however, an opposite sign change shows the existence of a local minimum in the signal. Using the following mapping, it would be possible to push down the positive part of the Hilbert transform to zero, while the negative part is mapped to a constant value:

$$y_2(t) = K_{2mag}\, y_0(t) \exp\left[\frac{-\lambda_{att}}{2}[1+\text{sign}(y_1(t))]y_1(t)\right], \quad (5)$$

in which K_{2mag} is the amplification coefficient, $y_0(t)$ is the filtered ECG signal and λ_{att} is the attenuation coefficient, which is a positive value and always $\lambda_{att} \geq 1$. The sign(.) operator is the sign function and $y_1(t)$ is the Hilbert transform of the filtered signal. According to Equation 5, it can be realized that for a

negative value of $y_1(t)$, $y_2(t) = K_{2mag}y_0(t)\exp(0) = K_{2mag}y_0(t)$, and the output would be the amplified version of the filtered signal. However, for positive values of $y_1(t)$, $y_2(t) = K_{2mag}y_0(t)\exp[-\lambda_{att}\ y_1(t)] \approx 0$. Thus, for negative values of the Hilbert transform, the filtered signal will be amplified, and for positive values of the Hilbert transform, the filtered signal will be mapped near zero. In the next step, using another nonlinear function, the negative values of the signal, $y_2(t)$, are eliminated as follows:

$$y_3(t) = K_{3mag}[1 + \text{sign}(y_2(t))]y_2(t), \tag{6}$$

where K_{3mag} represents the amplification coefficient. According to this equation, for a negative value of $y_2(t)$, signal $y_3(t)$ will be equal to zero; however, for positive values of $y_2(t)$, signal $y_3(t)$ will be amplified with the proportional factor, K_{3mag}. Afterwards, signal $y_3(t)$ is normalized and then re-amplified to define a proper subject-independent thresholding on the signal as follows:

$$y_4(t) = \exp\left[\frac{y_3(t)}{\max(y_3(t))}\right], \tag{7}$$

where $\max(y_3(t))$ represents the maximum value of the signal, $y_3(t)$.

Design of Adaptive Thresholding on Signal $y_4(t)$

Due to the variability of the morphology of QRS complexes in cases of arrhythmia, it will not be possible to detect all R-peaks using a fixed threshold value. For instance, if the threshold value is rather large relative to unity (unity is the minimum value of the signal, $y_4(t)$), the QRS complexes with a small $y_4(t)$ value will be located beneath the threshold line and, consequently, will not be detected. On the other hand, for values of the threshold highly close to unity, some waves will be detected in addition to QRS complexes, which will lead to a decrease in the algorithm accuracy, even if an improperly-detected QRS elimination algorithm is implemented. Accordingly, it seems that an adaptive thresholding is necessary and the algorithm would be more efficient. Suppose that the signal, $y_4(t)$, is divided into N number of identical segments with the values of μ_j and σ_j, respectively, for mean value and standard deviation of the signal segment in the jth interval ($j = 1, 2, \cdots, N$). For a threshold $\tau_j = \mu_j + \alpha\sigma_j$, where α is the adjustment coefficient ($0 < \alpha \leq 6$), one can calculate the corresponding suitable comparison threshold of each sample of signal $y_4(t)$ in each interval of $y_4(t)$. Thus, variability in the amplitude of signal $y_4(t)$, even in cases of large variation, will not cause significant errors in the proposed detection algorithm.

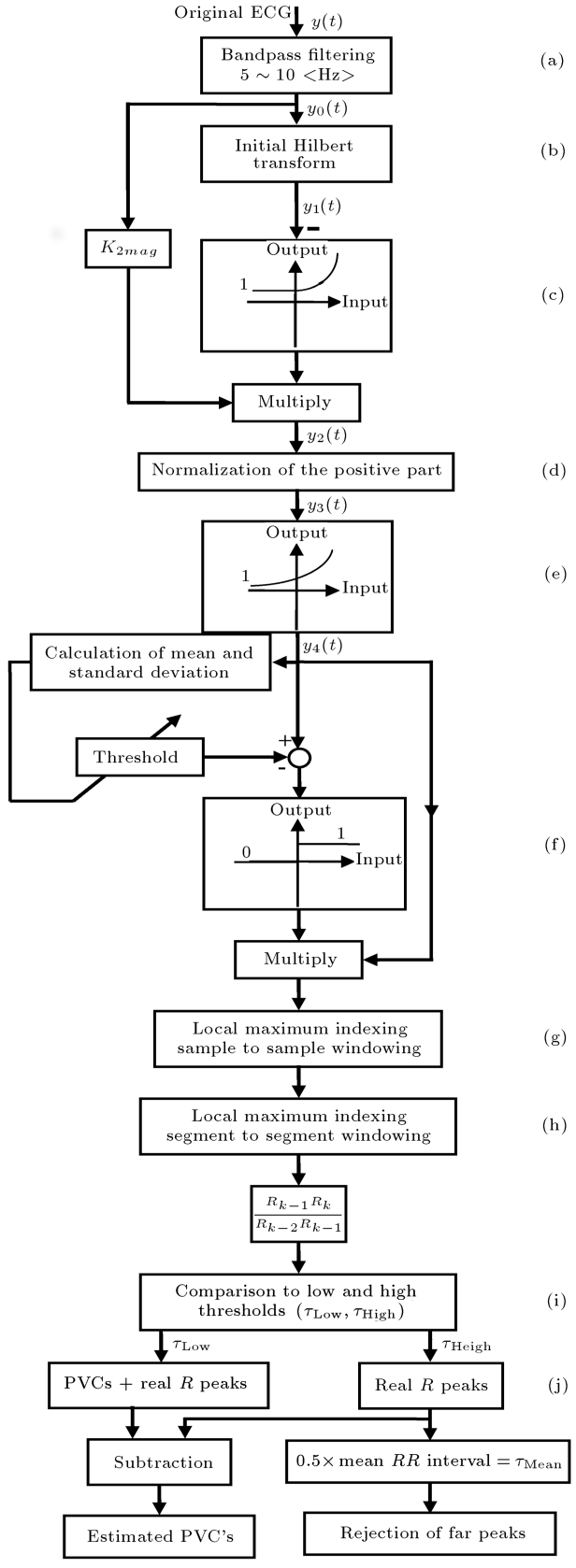

Figure 2. The block diagram of the MHT algorithm. From a general point of view this algorithm consists of 10 stages.

Sample to Sample Windowing: Selection of the Best Local Minimum

In this step, a window with an appropriate length of samples is selected and is slid on signal $y_5(t)$ from one sample to the next. Each time, the maximum value in the window and the corresponding index are calculated and all other points in the window are padded by zero. If moving forward, the new maximum entering the window is larger than the previous one, the previous maximum will be replaced by zero and the current maximum will play as a new QRS candidate. Finally, the output of the window will be called the best candidate for R-peak of the QRS complex.

Accordingly, using the calculated threshold, the signal, $y_5(t)$, can be obtained from signal, $y_4(t)$, as follows:

$$y_5(t) = \begin{cases} y_4(t) & y_4(t) \geq \tau(t) \\ 0 & y_4(t) < \tau(t) \end{cases} \tag{8}$$

Eventually, after applying a local search to the entire resulted signal, the proper candidates of QRS complexes will be obtained.

Elimination of Improperly-Detected Waves

In order to eliminate the QRS complexes with abnormal time distances from each other, suppose that index k represents the kth R-wave in the signal. Consequently, using a hypothesis test with the following test ratio;

$$L_R = \frac{R_{k+1} - R_k}{R_k - R_{k-1}}, \tag{9}$$

and a decision rule based on the following criterion;

$$\delta = \begin{cases} 1 & L_R \geq \tau_R \\ 0 & L_R < \tau_R \end{cases}, \quad \begin{matrix} 1 \equiv \text{ Holding } R_{k+1} \\ 0 \equiv \text{ Rejecting } R_{k+1} \end{matrix} \tag{10}$$

the $(k+1)$th R-wave with abnormal distance from the preceding R-wave will be eliminated. It should be noted that in Equations 9 and 10, τ_R is the rejection ratio and L_R is the decision ratio. In order to detect PVC beats, the factor, τ_R, should be chosen between 0.45 and 0.55 ($0.45 \leq \tau_R \leq 0.55$). However, for the values of τ_R between 0.55 and 0.70 ($0.55 \leq \tau_R \leq 0.70$), more accurate results will be obtained for R-wave detection. Finally, to remove much improperly-detected R-waves, it is assumed that the time sequence of RR-intervals (RR-tachogram) has a mean value, μ_C, and standard deviation, σ_C. Thus, if the equation $(R_k - R_{k-1}) \leq \mu_C + 3.5\sigma_C$ is held, the R_k peak will be rejected. The schematic block diagram of the MHT algorithm is depicted in Figure 2. Figure 3 also shows how the developed algorithm works to detect QRS complexes.

Design of Piecewise Polynomial Fitter (PPF)

The design of the Piecewise Polynomial Fitter (PPF) is based on the least squares method. In the PPF algorithm, the original signal is first divided into identical segments. In the next step, a pth-order polynomial ($3 \leq p \leq 15$, this interval is obtained empirically after numerous simulations) is fitted to each signal segment in the corresponding windows. Next, the discontinuities at the beginning and end of the intervals are eliminated using some simple calculations. The PPF algorithm has acceptable capability in cases of noise with non-stationary variance, low signal to noise ratios and colored noise. In this section, the design procedure of the PPF algorithm and the corresponding implementation method is first described and the related performance characteristics are then explained.

Piecewise Signal Isolation and Optimal Fitting

The principle of least squares has been studied extensively in systems identification [26] and estimation theory [27] textbooks. Consider the kth segment of a signal with length W_N such as $\{y(t)|t = 1+(k-1)W_N : kW_N\}$. A typical pth-order polynomial is supposed to be fitted to this signal segment as follows:

$$\hat{y}_k(t) - y_{0k} = \sum_{n=1}^{p} a_{nk}(t - t_{0k})^n, \tag{11}$$

where $\hat{y}_k(t)$ is estimation of the original signal in the kth interval, y_{0k} is the initial value of the interval, t_{0k} is the start time of the interval, and a_{nk} represents the polynomial coefficients that should be estimated using a BLUE algorithm.

Assuming the number of samples for each signal segment to be W_N, the following observation vector and time vector can be obtained for the kth segment of the signal:

$$\begin{cases} \mathbf{y}_{\text{obs},k} = \mathbf{y}[(1 + (k-1)W_N) : kW_N] \\ \mathbf{t}_{\text{obs},k} = \mathbf{t}[(1 + (k-1)W_N) : kW_N] \end{cases} \tag{12}$$

where $\mathbf{y}[m : n]$ represents the elements numbers m to n of a supposed vector, $\mathbf{y}$. Generally, in order to apply the BLUE algorithm to the problem, the observation and linear regression vectors must be in column and row formats, respectively. The observation vector, $\mathbf{Y}_k$, and time vector, $\mathbf{T}_k$, in the kth interval are obtained using Equation 12 as follows:

$$\begin{aligned} (\mathbf{Y}_k)_{W_N \times 1} &= \mathbf{y}_{\text{obs},k} - \mathbf{y}_{0k}, \\ (\mathbf{T}_k)_{W_N \times 1} &= \mathbf{t}_{\text{obs},k} - \mathbf{t}_{0k}, \end{aligned} \tag{13}$$

where $\mathbf{y}_{0k}$ and $\mathbf{t}_{0k}$ are the initial values of the kth interval and should be chosen so that the continuity

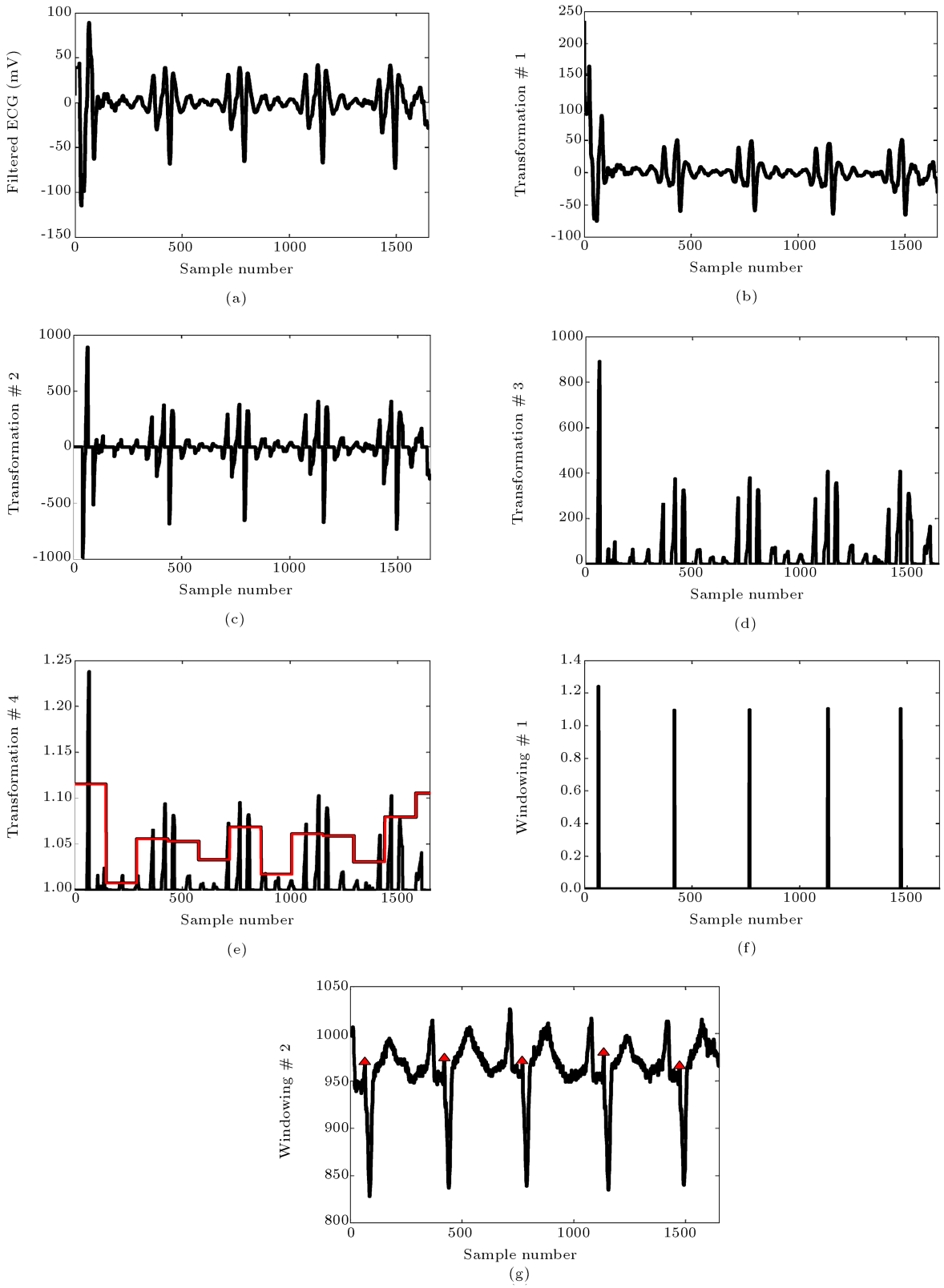

Figure 3. Graphical representation of the performance of MHT algorithm in the detection of QRS complexes. (a) Filtered ECG signal, (b) conventional Hilbert transform, (c) nonlinear mapping according to Equation 5, (d) padding zeros instead of negative values in signal obtained from previous section, (e) normalization and exponentially amplification of the preceding signal and application of the adaptive thresholding, (f) application of the sliding window to form the impulses originated from the best local maxima candidates and (g) application of a local search to the original signal centered on impulse indices obtained from stage (f).

of the entire estimated signal is guaranteed. In order to determine the matrix consisting of linear regression vectors, the time column vector $(\mathbf{T}_k)_{W_N\times 1}$ is substituted in the following matrix:

$$\mathbf{\Phi}_k = [\mathbf{T}_k, (\mathbf{T}_k)^{*2}, \cdots, (\mathbf{T}_k)^{*p}], \tag{14}$$

where the operator $(.)^{*m}$ increases each element of matrix $\mathbf{T}_k$ to the power of m. Suppose that in observation vector, $\mathbf{Y}_k$, the signal is embedded into an additive noise with covariance matrix, $\mathbf{\Omega}_k$. If so, it can be shown that the best linear unbiased estimation of unknown parameters in the presence of correlated noise is as follows [26]:

$$\boldsymbol{\theta}_k = (\mathbf{\Phi}_k^T \mathbf{\Omega}_k^{-1} \mathbf{\Phi}_k)^{-1} \mathbf{\Phi}^T \mathbf{\Omega}_k^{-1} \mathbf{Y}_k, \tag{15}$$

in which, $\boldsymbol{\theta}_k$ includes the parameters of the polynomial in an ascending fashion, i.e. $\boldsymbol{\theta}_k = [a_{1k}, a_{2k}, \cdots, a_{pk}]^T$. The details to derive this equation, as well as the corresponding exhaustive explanation of this type of estimation, can be found in identification textbooks [26,27]. Presenting a simple example, it is shown how to apply the continuity condition to the beginning and end of each interval. Consider a sequence consisting of 17 samples with window length $W_N = 12$ as depicted in Figure 4.

In this figure, the solid line represents the original signal, which should be estimated by the PPF algorithm, and the dashed lines illustrate polynomials fitted to the signal in each segment. As observed in this figure, the estimated signal is not appropriately fitted to the original signal at end point A (end effect 1). To solve the problem, it is assumed that the corresponding polynomial of each interval is fitted to W'_N number of samples where $W'_N = W_N + W_{aug}$ and W_{aug} is the number of samples borrowed from the next adjacent window augmented to vector $\mathbf{T}_k$. According to Equation 12, vectors $\mathbf{y}_{\text{obs},k}$ and $\mathbf{t}_{\text{obs},k}$ are obtained

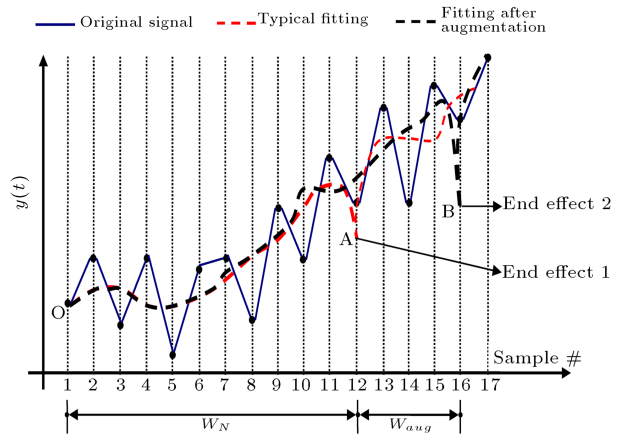

Figure 4. Schematic representation of end effects in the PPF algorithm and extra samples augmentation.

as follows:

$$\mathbf{y}_{\text{obs},k} = \mathbf{y}\lfloor(1+(k-1)W_N) : kW_N + W_{aug}\rfloor,$$

$$\mathbf{t}_{\text{obs},k} = \mathbf{t}[(1+(k-1)W_N) : kW_N + W_{aug}]. \tag{16}$$

In this way, the polynomial parameters are determined from Equation 15 and the corresponding signal in this interval can be estimated as follows:

$$\mathbf{T}_k = \mathbf{t}[(1+(k-1)W_N) : kW_N + 1] - t_{0k}, \tag{17}$$

$$\mathbf{\Phi}_k = [\mathbf{T}_k, (\mathbf{T}_k)^{*2}, \cdots, (\mathbf{T}_k)^{*p}]_{(W_N+1)\times p}, \tag{18}$$

$$\hat{\mathbf{y}}(t) = \mathbf{\Phi}_k \boldsymbol{\theta}_k + y_{0k}. \tag{19}$$

Applying this method, the end effect 2 (end point B) is arisen out of the interval. However, only samples from the beginning to the end of segment (W_N) are considered as the estimated signal. Therefore, the end effects are eliminated.

It should be noted that the signal in this interval is estimated using a rather high-order polynomial, which has low generalization power for the estimation in endpoints. Choosing some samples from interval $k+1$ to proceed the last sample of interval k results in more accurate estimation for the endpoint and, consequently, a smoother estimation is obtained for the original signal in interval k. The last point of interval k and the corresponding time will be used as the initial conditions for the next interval, $k+1$, i.e.,

$$\begin{cases} y_{0(k+1)} = \hat{\mathbf{Y}}_k(\text{end}) \\ t_{0(k+1)} = \mathbf{T}_k(\text{end}) \end{cases} \tag{20}$$

Finally, in order to conduct estimation in interval $k+1$, the linear regression matrix and the observation vector should be obtained from Equation 19 and the first elements in the vectors $\mathbf{t}_{\text{obs},(k+1)}$ and $\mathbf{y}_{\text{obs},(k+1)}$ should be replaced by $y_{0(k+1)}$ and $t_{0(k+1)}$, respectively.

Generally, it should be noted that window length W_N depends upon the sampling frequency, frequency contents of the original signal, the order of the polynomial, and noise power. After fulfillment of numerous simulations, it is empirically concluded that this performance would be highly improved if the following criterion was used:

$$W_N = \lambda \min\left\{\frac{1}{4}F_S, 3f_{dom}, 15p\right\}, \tag{21}$$

where, F_S represents the sampling frequency, f_{dom} is the largest frequency existing in the signal, and p is the order of the polynomial. Also, λ is a proportion coefficient that varies between 1 and 1.5 ($1 \le \lambda \le 1.5$), and depends on the approximate standard deviation of the noise. In this study, for the values of noise standard deviation less than 4 ($\sigma_N < 4$), λ is set to 1 ($\lambda = 1$), and for the values of noise standard deviation more than 4($\sigma_N > 4$), it was considered equal to 1.5 ($\lambda = 1.5$).

Classification of Data and Feature Space Dimension Reduction

Radial Basis Function (RBF) Based Support Vector Machine (SVM) Classifier

In this work, RBF-SVM is implemented as the arrhythmias classification method. According to the Vapnik formulation [28], if couple $(\mathbf{x}_i, \delta(\mathbf{x}_i))$ (in which $\delta(\mathbf{x}_i)$ is class function, $i = 1, \cdots, N$) describing data elements and their corresponding categories that are linearly separable in the feature space, then the margin of classes can be obtained as follows:

$$\mathbf{f}(\mathbf{x}) = \mathbf{w}^T \boldsymbol{\varphi}(\mathbf{x}) + \mathbf{b}, \tag{22}$$

where $\mathbf{w}$ is weight vector, $\mathbf{b}$ is bias term and the condition $\mathbf{f}(\mathbf{x}_i)\delta(\mathbf{x}_i) > 0$ holds. On the other hand, if train data is not linearly separable in the feature space to find a suitable separating hyper plane, the following constrained optimization problem should be solved:

$$\text{CoF}(\mathbf{w}, \xi) = \frac{1}{2}\|\mathbf{w}\|^2 + C\sum_{j=1}^{N} \xi_j,$$

s.t.

$$\delta(\mathbf{x}_i)(\mathbf{w}^T \boldsymbol{\varphi}(\mathbf{x}_i) + \mathbf{b}) \geq 1 - \xi_i,$$

$$i = 1, \cdots, N, \tag{23}$$

where CoF is the cost function. Solving this equation yields the separating hyper plane. In this equation, C is called the regularization parameter that generates a trade-off between the hyper plane margin and classification error, and ξ_i is stack parameter corresponding to $\mathbf{x}_i$. By introducing Lagrange multipliers as:

$$\text{CoF}(\alpha) = \sum_{j=1}^{N} \alpha_j - \frac{1}{2}\sum_{i=1}^{N}\sum_{j=1}^{N} \alpha_i \alpha_j \delta(\mathbf{x}_i)\delta(\mathbf{x}_j)K(\mathbf{x}_i, \mathbf{x}_j),$$

s.t.

$$\sum_{j=1}^{N} \alpha_j \delta(\mathbf{x}_j) = 0,$$

$$0 \leq \alpha_j \leq C, \tag{24}$$

where $K(\mathbf{x}_i, \mathbf{x}_j)$ is the kernel function obtained from the following equation:

$$K(\mathbf{x}_i, \mathbf{x}_j) = \boldsymbol{\varphi}^T(\mathbf{x}_i)\boldsymbol{\varphi}(\mathbf{x}_j). \tag{25}$$

For example, $K(\mathbf{x}_i, \mathbf{x}_j) = (\mathbf{x}_i^T \mathbf{x}_j + 1)^\lambda$ is polynomial kernel of degree λ and $K(\mathbf{x}_i, \mathbf{x}_j) = \exp(-\gamma\|\mathbf{x}_i - \mathbf{x}_j\|^2)$ is the RBF kernel. In Equation 20, if $\alpha_i > 0$, $\mathbf{x}_i$s are called support vectors. In specific cases, if $\alpha_i = C$, $\mathbf{x}_i$s are bounded support vectors and if $0 < \alpha_i < C$, $\mathbf{x}_i$s will be called unbounded support vectors. To solve the constrained Equation 20, several approaches can be found in the literature [28]. After solving Equation 20, the decision function $\mathbf{f}(\mathbf{x})$ is obtained as follows:

$$\mathbf{f}(\mathbf{x}) = \sum_i \alpha_i \delta(\mathbf{x}_i) K(\mathbf{x}_i, \mathbf{x}) + \mathbf{b},$$

$$\mathbf{w} = \sum_j \delta(\mathbf{x}_j)\alpha_j \boldsymbol{\varphi}(\mathbf{x}_j), \tag{26}$$

and margin $\boldsymbol{\Lambda}$ is obtained as:

$$\boldsymbol{\Lambda} = \frac{1}{\|\mathbf{w}\|} \frac{1}{\sqrt{\sum_i \sum_j \delta(\mathbf{x}_i)\delta(\mathbf{x}_j)\alpha_i \alpha_j K(\mathbf{x}_i, \mathbf{x}_j)}}. \tag{27}$$

More details about fundamental concepts of SVM can be found in [28].

Feature Space Dimension Reduction via Principal Component Analysis (PCA)

Suppose that $\mathbf{F}_{\text{Arr}} = [\mathbf{f}_1, \cdots, \mathbf{f}_N]$ is a matrix consisting of feature vectors $(\mathbf{f}_j)_{12\times 1}$, $j = 1, \cdots, N$, and it is aimed to reduce the dimension of $\mathbf{F}_{\text{Arr}}$ and reconstruct a matrix $\mathbf{G}_{\text{Arr}} = [\mathbf{g}_1, \cdots, \mathbf{g}_N]$, in which $(\mathbf{g}_j)_{p\times 1}$, $j = 1, \cdots, N$ and $p \leq 12$. Using the following linear orthonormal projection:

$$\mathbf{g} = \boldsymbol{\Omega}^T \mathbf{f} + \mathbf{u}, \tag{28}$$

where $\boldsymbol{\Omega}_{12\times p}$ is the weight matrix and $\mathbf{u}_{p\times 1}$ is the offset vector, and by application of linear back projection, the estimation of vector $\mathbf{f}$, i.e. $\hat{\mathbf{f}}$, is obtained as follows:

$$\hat{\mathbf{f}} = \boldsymbol{\Omega}(\mathbf{g} - \mathbf{u}). \tag{29}$$

This equation is obtained based on the orthonormal characteristics of the weight matrix, $\boldsymbol{\Omega}$. To calculate optimal weight matrix $\boldsymbol{\Omega}$ and offset vector $\mathbf{u}$, a square error structure is defined as:

$$\varepsilon(\boldsymbol{\Omega}, \mathbf{u}) = \frac{1}{N}\sum_{k=1}^{N} \mathbf{f}_k^T \hat{\mathbf{f}}_k, \tag{30}$$

and $(\boldsymbol{\Omega}, \mathbf{u})$ is the optimal solution of the following constrained optimization equation:

$$(\boldsymbol{\Omega}, \mathbf{u}) = \underset{(\boldsymbol{\Omega}_0, \mathbf{u}_0)}{\text{Arg min}}[\varepsilon(\boldsymbol{\Omega}_0, \mathbf{u}_0)],$$

s.t.

$$\boldsymbol{\Omega}^T \boldsymbol{\Omega} = \mathbf{I}, \tag{31}$$

where condition $\boldsymbol{\Omega}^T\boldsymbol{\Omega} = \mathbf{I}$ imposes an orthonormality constraint to the optimization problem. To solve Equation 17, several methods, such as Cholesky decomposition and linear algebra methods, have already been

developed [28]. The main role of PCA application is to reduce the feature space dimension, so that training time and computational burden decreases significantly. However, for low dimension feature vectors, such as those in this study, implementation of PCA makes no considerable improvement in training accuracy and computational burden.

FEATURE EXTRACTION USING A RISK SCORING MODEL DEVELOPED FOR PREDICTION OF CARDIOGENIC SHOCK INCIDENCE

Cardiogenic Shock and Risk Scoring Model

Cardiogenic shock is a certain state in which slight systemic cardiac output leads to tissue hypoxia. For values of cardiac index less than or equal to 2.2 liter/min/m^2 (or 1.8 liter/min/m^2 according to physiologists) cardiogenic shock will occur. From the blood pressure perspective, a systolic blood pressure less than 80 or 90 mmHg can be a symptom of shock syndrome. However, it is proven that hypotension is not the only cause of shock occurrence. The hemodynamic parameters which contribute significantly to the detection or prediction of shock are namely heart rate, right atrial pressure, right ventricle systolic/diastolic pressure, pulmonary artery pressure, left atrial pressure, left ventricle systolic/diastolic pressure, aortic pressure, cardiac output, cardiac index, stroke volume, left ventricle diastolic volume, ejection fraction, systemic resistance, total pulmonary resistance, stroke work index of the left ventricle and baseline cardiac power out. Generally, a considerable decrease will occur in the systemic tissue perfusion during cardiogenic shock. The main consequences of cardiogenic shock include renal failure, changes in pulmonary function, changes in skeletal muscle, dysfunction in the gastrointestinal system, decrease in blood pressure and blood volume, and damage to the brain. The schematic diagram of cardiogenic shock is illustrated in Figure 5 in which successive MI cause the cardiac pumping level to descend to below the rest baseline. In this way, cardiogenic shock occurs that can rapidly lead to death [29].

In this section, a shock predictor model [6] is introduced in which factors such as age, heart rate, SBP, DBP, weight, and some other clinical features namely miscellaneous factors are incorporated. At the first step, based on clinical data and the significance of the factor under study, a score is allocated to each feature. For instance, age is a variable strongly increasing the probability of cardiogenic shock or Mean Arterial Pressure (MAP), which is derived from SBP and DBP, and which is considerably associated with the occurrence of cardiogenic shock. Therefore, a high

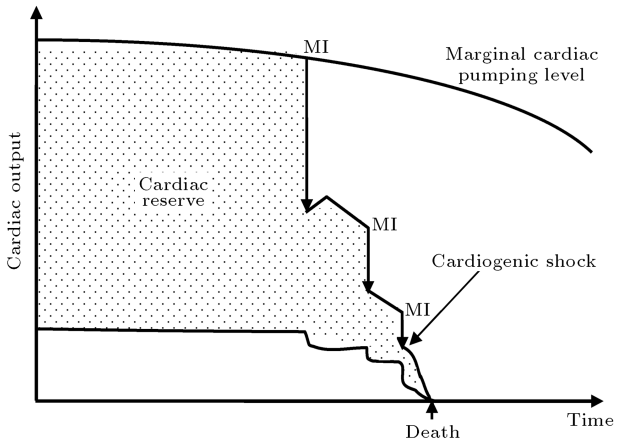

Figure 5. The diagram of cardiogenic shock occurrence after cumulative MIs showing deterioration of cardiac pumping capability [25].

score should be allotted to these factors. Afterwards, a total score is calculated as the sum of the scores assigned to each factor. Finally, it would be possible to predict the probability of cardiogenic shock for the patient under consideration. As a case in view, consider a 71-year-old 60-kg female with a history of hypertension who presents with a systolic blood pressure of 126 mmHg, a diastolic blood pressure of 64 mmHg and a heart rate of 123 beats/min. According to the model of Hasdai et al., this patient would have a total score of $37 + 17 + 39 + 5 + 10 + 5 + 8 + 17 + 3 + 2 + 5 = 148$. This score corresponds to a predicted probability of 30% for cardiogenic shock [6].

Feature Selection for Detection and Prediction of Cardiogenic Shock Using Hasdai et al. Risk Model

For Computer Implementation of the Hasdai et al. model, a RBF-SVM network is trained using information obtained from their original work [6]. The purpose of using the RBF-SVM was to consider the mutual influence of parameters in the evaluation of shock probability for which a RBF-SVM network is implemented. Using this network, it will be possible to incorporate the possible mutual influences between risk parameters to the calculation of shock occurrence probability.

According to Figure 6, inputs such as HR, SBP, DBP, age, gender and weight are included in the input layer and are incorporated in exponential kernel functions. The structure of this network is illustrated in Figure 6. For each of the parameters, HR, SBP, DBP, age, gender and weight, an exponential kernel function is supposed. The range of exponential kernel functions parameters are illustrated in the next section.

The resulted RBF-SVM classifier is erected in a

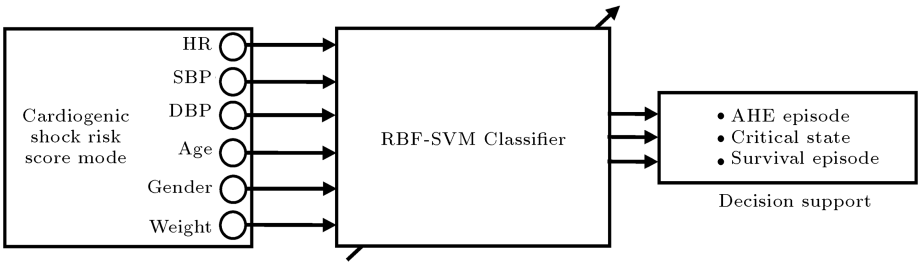

Figure 6. The RBF-SVM structure used for cardiogenic shock predictor based on HR, SBP, DBP, age, gender and weight.

C++ environment, according to Figure 6, to calculate the risk of cardiogenic shock occurrence and classify the present spontaneous status. As already stated, the variable describing shock in the Hasdai et al. model can be obtained using an equation similar to the following:

$$\mathbf{X}_{\mathrm{TOT}} = \mathbf{X}_{\mathrm{AGE}} + \mathbf{X}_{\mathrm{HR}} + \mathbf{X}_{\mathrm{SBP}} + \mathbf{X}_{\mathrm{DBP}} + \mathbf{X}_{\mathrm{WGT}} + \mathbf{X}_{\mathrm{MIL}} + \mathbf{X}_{\mathrm{TRT}} + \mathbf{X}_{\mathrm{KLP}} + \mathbf{X}_{\mathrm{MSC}}. \quad (32)$$

More details about the Hasdai et al. risk score model can be found in [6]. As understood from Equation 22, the total sum of scores will yield the shock overall index and, using a final mapping, the percentage of the probability of shock occurrence can be calculated [6].

In Figure 7, a generic example of the risk factor and its classification bounds obtained applying the Hasdai et al. model is shown. As seen in this figure, the spontaneous value of risk factor is used as a metric to allocate the probability of cardiogenic shock occurrence.

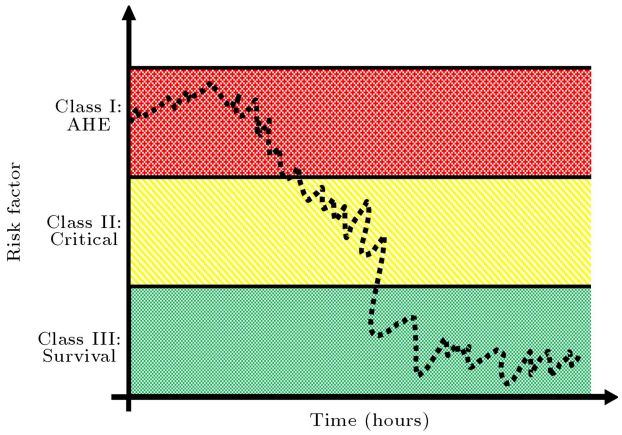

Figure 7. A generic trend of risk factor calculated using smoothed SBP, DBP, HR and some other miscellaneous factors. Corresponding survival, critical and AHE classes are also illustrated.

Technical Descriptions of Employed Databases

The MIT-BIH Arrhythmia Database

The MIT-BIH Arrhythmia Database contains 48 half-hour excerpts of two-channel ambulatory ECG recordings, obtained from 47 subjects studied by the BIH Arrhythmia Laboratory. Twenty-three recordings were chosen at random from a set of 4000 24-hour ambulatory ECG recordings collected from a mixed population of inpatients (about 60%) and outpatients (about 40%) at Boston Hospital. The remaining 25 recordings were selected from the same set to include less common but clinically significant arrhythmias that would not be well-represented in a small random sample. The recordings were digitized at 360 samples per second per channel with 11-bit resolution over a 10 mV range. Two or more cardiologists independently annotated each record. Disagreements were resolved to obtain the computer-readable reference annotations for each beat (approximately 110,000 annotations in all) included with the database [30].

The TWA Database

This database has been assembled for the PhysioNet/Computers in Cardiology Challenge 2008. It contains 100 multichannel ECG records sampled at 500 Hz with 16 bit resolution over a ± 32 mV range. The subjects include patients with myocardial infarctions, transient ischemia, ventricular tachyarrhythmias, and other risk factors for sudden cardiac death, as well as healthy controls and synthetic cases with calibrated amounts of T-wave Alternans [30].

The QT Database

The QT Database includes ECGs which were chosen to represent a wide variety of QRS and ST-T morphologies in order to challenge QT detection algorithms with real-world variability. The records were chosen primarily from among existing ECG databases including the MIT-BIH Arrhythmia Database, the European Society of Cardiology ST-T Database, and several other ECG databases collected at Boston's Medical Center. All records were sampled at 250 Hz [30]. Those which were not originally sampled at that rate were converted using the MIT Waveform Database Software Package [30].

High Resolution DAY Hospital Database

The high-resolution Holter Database of DAY hospital contains 24-hour 3-lead records of about 150 patients, including diverse ECG arrhythmias, such as BBB, PVC, PAC, myocardial infarction, heart failure, ischemia and T-wave alternans. The sampling frequency of this database is 1000 Hz with 32-bits of resolution [31]. The electrodes of each holter are attached to the subjects' chest skin surface at positions 1, 3, 5 via suitable vacuum cups.

Computers in Cardiology Challenge 2009 (Files Chosen from MIMIC II) Database

The MIMIC II project has collected data from about 30000 ICU patients to date. MIMIC II patient records contain most of the information that would appear in a medical record (such as results of laboratory tests, medications, and hourly vital signs). About 5000 of the records also include physiologic waveforms (typically including ECG, blood pressure and respiration, and often other signals as well) and time series that can be observed by the ICU staff. The intent is that a MIMIC II record should be sufficiently detailed to allow its use in studies that would otherwise require access to an ICU, e.g. for basic research in intensive care medicine, or for development and evaluation of diagnostic and predictive algorithms for medical decision support. The challenge dataset consists of selected patient records from the MIMIC II Database. In the training set, the records include all available data before and after $\mathbf{T}_0$. In the test sets, the records are truncated at $\mathbf{T}_0$; the data recorded after $\mathbf{T}_0$ in each case will be made available for study only after the conclusion of the challenge. Not all MIMIC II records include all data elements needed for this challenge. Records chosen for the challenge dataset include, at a minimum, at least 10 hours of data before $\mathbf{T}_0$, and at least one hour of data after $\mathbf{T}_0$. (As noted, data collected after $\mathbf{T}_0$ for the test set records will be withheld until after the conclusion of the challenge in September, 2009.) Most MIMIC II records are significantly longer, and many include a week or more of data. ECG and Arterial Blood Pressure (ABP) signals are sampled at 125 Hz. Records in the training set may include one or two additional signals, and those in the test set may include as many as six additional signals. (Note, however, that two records in the training set do not include these signals.) Time series of vital signs are sampled once per minute (in the training set) and once per second (in the test sets). These include heart rate and mean, systolic, and diastolic ABP. Most records include a variety of additional vital-signs time series, most often including respiration rate and SpO_2. Clinical data are entered into the ICU medical information systems (records of observations, measurements and interventions performed in the ICU). These include intravenous medications and fluids as well as other medications administered. Note, however, that some of this information is manually entered by the ICU staff at times when it is possible to do so without compromising patient care, so the associated timestamps may be imprecise. Results of laboratory tests, records of medications ordered, and other data gathered in the hospital but outside the ICU are recorded. MIMIC II records meeting the criteria above are assigned to a group (H or C) and a subgroup (H1, H2, C1 or C2). Records in group H contain an episode of acute hypotension beginning during the forecast window (the one-hour period following $\mathbf{T}_0$). Records in subgroup H1 come from patients who received pressor medication. Records in subgroup H2 come from patients who did not receive pressor medication (i.e. those in group H but not in subgroup H1). Records in group C contain no episodes of acute hypotension within the forecast window. Records in subgroup C1 come from patients with no documented acute hypotensive episodes at any time during their hospital stay. Records in subgroup C2 come from patients who had AHE before or after the forecast window (i.e. those in group C but not in subgroup C1). The training set consists of 60 records (including data after $\mathbf{T}_0$): 15 from subgroup H1 (AHE treated with pressors), 15 from subgroup H2 (AHE not treated with pressors), 15 from subgroup C1 (no AHE) and 15 from subgroup C2 (AHE outside the forecast window) [30].

Estimation of MAP and Its Dropping Regimes

Because the MIT-BIH Database includes long time signals (more than 30 hours), the outputs of BPMHT and ECGMHT algorithms are averaged in one-minute intervals. If so, the size of data to be processed will be 1/125 the size of the original data (the sampling frequency of MIMIC II Database is 125 Hz). Finally, MAPDR calculations are conducted using the average data.

In order to find MAPDRs, a window with length W_{DR} is the first slide sample to sample the smoothed averaged waveform $\mathbf{Y}_{bp,sm}$ obtained from the PPF algorithm, i.e. $\mathbf{Y}_{bp,sm} = \mathrm{PPF}(\mathbf{Y}_{bp,\mathrm{orig}})$. The MAP waveform, $\mathbf{Y}_{bp,\mathrm{orig}}$, is calculated using SBP and DBP pulses as follows [1]:

$$\mathbf{Y}_{bp,\mathrm{orig}} \approx \frac{\mathbf{Y}_{\mathrm{SBP}} + 2\mathbf{Y}_{\mathrm{DBP}}}{3} \ (\mathrm{mmHg}), \tag{33}$$

where $\mathbf{Y}_{\mathrm{SBP}}$ and $\mathbf{Y}_{\mathrm{DBP}}$ are SBP and DBP vectors. The window length, W_{DR}, is equal to the number of samples as long as 30 minutes. Each time, the Drop Index (DI), MAPDR, is calculated as follows. First, the signal segment in the kth window is obtained as:

$$\mathbf{Y}_{\mathrm{seg},k} = \mathbf{Y}_{bp,sm}(k : k + W_{\mathrm{DR}}). \tag{34}$$

In the next step, the derivative of vector $\mathbf{Y}_{\text{seg},k}$ is calculated with respect to time as follows:

$$\dot{\mathbf{Y}}_{\text{seg},k} = \text{diff}(\mathbf{Y}_{\text{seg},k}), \tag{35}$$

where operator diff(.) represents the difference between the present sample and the previous one. The aim of this study is to detect intervals with MAP at or below 60 mmHg descending continuously. To this end, all samples of vector $\dot{\mathbf{Y}}_{\text{seg},k}$ in a window are summed up. If this total sum is always negative when sliding the window forward, it would be a marker of MAPDR. On the other hand, an increase in the total sum indicates an ascending trend for MAP. Therefore:

$$\text{DI}(k) = \sum_{n=1}^{W_{\text{DR}}} \dot{\mathbf{Y}}_{\text{seg},k}(n), \qquad \text{MAP} \leq 60 \quad \text{mmHg}. \tag{36}$$

From the resulted signal, DI, negative parts with high duration should be highly considered. Thus:

$$\text{MAPDR} = 0.5[1 - \text{sign}(\text{DI})], \tag{37}$$

where index MAPDR represents a signal with a value of 1 for MAPDR and zero for the ascending trend in the MAP signal. If the drop index descends continuously for 90% of the window length when moving forward, a dropping regime will be assigned to that specific period of time.

Normalization of Data

Suppose that the vector $\mathbf{X}$ has sample mean μ and sample variance σ^2, then the normalized vector, $\mathbf{X}_{\text{Norm}}$, processing zero mean and unit variance, is obtained from the following simple transformation:

$$\mathbf{X}_{\text{Norm}} = \frac{\mathbf{X} - \mu}{\sigma}. \tag{38}$$

Normalization of the shock probability diagram helps us obtain a comprehensive comparative criterion for all subjects.

Simulation of QRS and Pulse Pressure Detectors

Validation of MHT Algorithm for the Detection of QRS Complexes (ECGMHT)

Numerous databases with different sampling frequencies and signal to noise ratios are used in this study to validate the performance of the proposed detection algorithm. To validate the QRS detection and delineation algorithm, MITDB (F_s = 360 Hz), TWADB (F_s = 500 Hz), EDB (F_s = 250 Hz), QTDB (F_s = 250 Hz) and also high resolution Holter data (MEDSET®-1000 Hz, 3-Channel, 32-bits) that contain annotation files are used (CHECK#0). It should be noticed that in confusing situations, results were delivered to the cardiologist and, accordingly, the detection algorithm was revalidated (CHECK#1). In cases of QRS with very abnormal morphologies, the results were also checked by some residents (CHECK#2).

The results of the application of the MHT method are shown in Tables 1 to 5 with the average values of 99.80% and 99.85% for sensitivity and positive prediction, respectively. The False Negative (FN) occurs when the algorithm fails to detect a true beat (actual QRS) conducted in the corresponding annotation file of the MIT-BIH record, and a False Positive (FP) indicates a false beat detection. Sensitivity (Se) and positive prediction ($P+$) [13] are calculated straightforwardly as follows:

$$\text{Sensitivity } (\%) = \frac{\text{TP}}{\text{TP} + \text{FN}}\%, \tag{39}$$

$$\text{Positive predictivity}(\%) = \frac{\text{TP}}{\text{TP} + \text{FP}}\%. \tag{40}$$

Two graphs will be representing the output of the MHT algorithm. The first graph depicts the output of the applied transforms as well as adaptive thresholds in each window (see Figure 2 (sections e and g)). Observing these figures, one can assess the accuracy of the results and the corresponding parameter values. For appropriate values of thresholds, acceptable results would be expected from the method; however, for very low values of thresholds, some waves other than the actual R-waves will be improperly detected. Furthermore, for high values of thresholds, some QRS complexes will not be detected correctly. In these two cases, the parameter values should be re-adjusted and the algorithm should be re-applied to the original signal so that acceptable results are obtained. It should also be noticed that the window length can be adjusted as another parameter, so that more accurate results are gained from the algorithm. This window length will generally be equal to 550 $\sim$ 700 milliseconds (this value obtained from practical application of the MHT algorithm) for cases of PVC not observed in the original signal. However, if PVCs exist in the original ECG, the parameter value of 500 $\sim$ 550 milliseconds will lead to better results. Finally, in the second figure, the corresponding R-wave in the original signal is represented. The annotation files of the MIT-BIH Arrhythmia Database include information about normal beats (N), PVCs (V) and changes in the signal quality ($\sim$). The results of the MHT algorithm are compared to this information for the purposes of validation and the outcomes, including True Positive (TP), False Negative (FN) and False Positive (FP) values, are calculated and presented in Tables 1 to 5. The resulted values for sensitivity and

Table 1a. Evaluation of the ECGMHT algorithm performance on some records of the MIT-BIH Arrhythmia database.

MIT-BIH Record	Total # of Beats	FP	FN	FP+FN	FP+FN (%)	Se (%)	$P+$ (%)
100	2273	0	0	0	0	100	100
108	1765	8	13	21	1.19	99.3	99.5
207	1862	13	22	35	1.88	98.8	99.3
213	3251	0	11	11	0.34	99.7	100
217	2209	0	0	0	0	100	100

Table 1b. Performance evaluation of several QRS detection algorithms: Application to MITDB.

Detection Algorithm	# of Annotations	TP	FP	FN	Error (%)	Se (%)	$P+$ (%)
This Study	109428	109215	160	213	0.34	99.80	99.85
Ghaffari et al. [31]	109428	109327	129	101	0.21	99.91	99.88
Martinez et al. [32]	109428	109208	153	220	0.34	99.80	99.86
Li et al. [33]	104182	104070	65	112	0.17	99.89	99.94
Hamilton et al. [34]	109267	108927	248	340	0.54	99.69	99.77
Pan et al. [35]	109809	109532	507	277	0.71	99.75	99.54
Moody et al. [36]*	109428	107567	94	1861	1.79	98.30	99.91

*: Also called ARISTOTLE software

Table 2. Performance evaluation of QRS detection algorithms: Application to QTDB.

Detection Algorithm	# of Annotations	TP	FP	FN	Error (%)	Se (%)	$P+$ (%)
This Study	86892	86819	94	73	0.19	99.92	99.89
Ghaffari et al. [31]	86892	86845	79	47	0.15	99.94	99.91
Martinez et al. [32]	86892	86824	107	68	0.20	99.92	99.88
Moody et al. [36]	86892	84458	459	2434	3.33	97.2	99.46

Table 3. Performance evaluation of QRS detection algorithms: Application to EDB.

Detection Algorithm	# of Annotations	TP	FP	FN	Error (%)	Se (%)	$P+$ (%)
This Study	787103	783992	4134	3111	0.92	99.60	99.47
Ghaffari et al. [31]	78103	784168	4016	2980	0.72	99.69	99.68
Martinez et al. [32]	787103	784059	4077	3044	0.90	99.61	99.48
Moody et al. [36]	787103	748468	10405	38635	6.23	95.09	98.63

Table 4. Performance evaluation of QRS detection algorithms: Application to TWADB.

Detection Algorithm	# of Annotations	TP	FP	FN	Error (%)	Se (%)	$P+$ (%)
This Study	11789	11760	24	29	0.45	99.75	99.80
Ghaffari et al. [31]	11789	11776	18	13	0.26	99.89	99.84

Table 5. Performance evaluation of MHT algorithm on high-resolution 24-hour Holter database including a vast spectra of heart rates (CHECK#0,CHECK#1).

Holter Record	# of Beats	# of PVC*	# of PAC**	TP	FP	FN	Error (%)	Se (%)	$P+$ (%)
PVCDAT 1-5	188531	53	0	52	0	1	1.89	98.11	100
PVCDAT 6-10	174515	148	0	147	1	1	1.35	99.32	99.32
PVCDAT 11-15	179428	312	0	310	2	2	1.28	99.36	99.36
PVCDAT 16-20	189749	1253	0	1247	9	6	1.20	99.52	99.28
PACDAT 1-4	163934	0	323	322	1	1	0.62	99.69	99.69
PACDAT 5-8	157635	0	611	610	1	1	0.33	99.83	99.83
PACDAT 9-12	107891	0	5513	5505	12	8	0.36	99.85	99.78
PAVDAT 1-4	114204	164	22	185	2	1	1.61	99.46	98.93
PAVDAT 5-8	171315	237	52	287	2	2	1.38	99.31	99.31
PAVDAT 9-12	197591	1153	219	1367	9	5	1.02	99.66	99.35
PAVDAT 13-15	108344	1636	788	2419	14	5	0.78	99.79	99.42
Total	1,753,137	4956	7528	12451	53	33	0.69	99.73	99.58

*: Premature Ventricular Contraction.

**: Premature Atrial Contraction.

positive prediction are acceptable results in the context of QRS detection [25].

Characterization of End-Systolic and End-Diastolic Pulses of the Arterial Blood Pressure (ABP) Waveform Using the MHT Algorithm (BPMHT)

In this section, in order to generalize the application of the MHT algorithm, it is applied to ABP waveforms of all 18 subjects of the MIT-BIH Polysomnographic Database [30], and the corresponding end-systolic and end-diastolic pulses of the ABP waveform are extracted.

The results of the algorithm applied to blood pressure waveforms are shown in Table 6. The mean values of 99.80% and 99.86% are obtained for sensitivity and positive prediction, respectively.

Cardiogenic Shock Detection and Occurrence Prediction Using the Trained SVM Classifier

In this section, a signal with a chirp frequency is embedded into a colored noise. Then, the variance of the sequence of white noise is increased with a specific increment and the estimated signal is extracted. The standard deviation of the difference between the estimated signal and the original signal is represented in Figure 8. As seen in Figure 8b, the

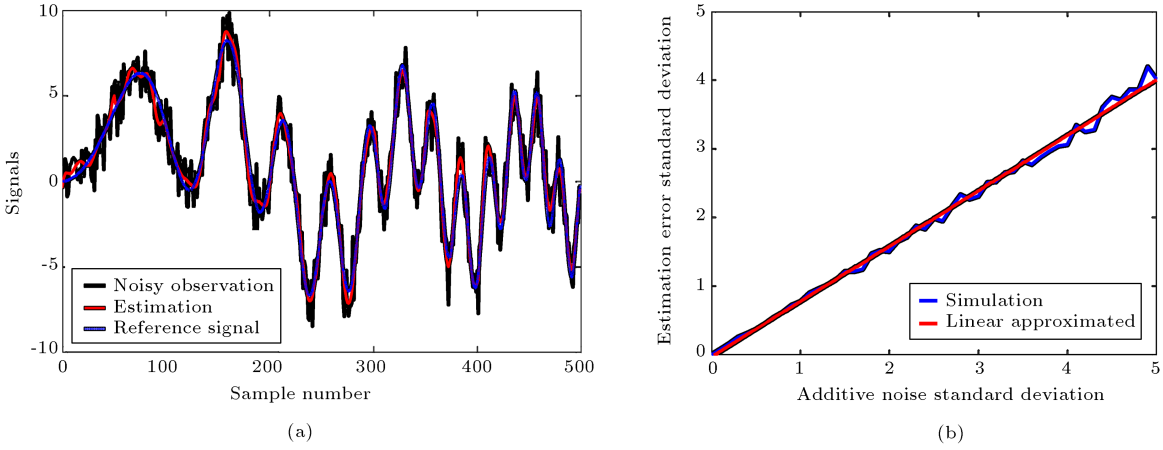

Figure 8. (a) Graphical representation of the performance of PPF algorithm: Solid lines are noisy observation as well as signal estimation and dashed line represents the reference signal. (b) Standard deviation of estimation error versus standard deviation of the i.i.d. noise sequence.

Table 6. Application of the MHT algorithm to the MIT-BIH Polysomnographic database and obtained results. A total of 650000 samples are chosen for each record.

MIT-BIH Record	Total # of Beats	FP	FN	FP+FN	FP+FN (%)	Se (%)	$P+$ (%)
slp01a	2797	0	5	5	0.18	99.82	100
slp01b	2834	2	3	5	0.18	99.89	99.93
slp02a	4028	0	15	15	0.37	99.63	100
slp02b	3408	0	7	7	0.21	99.79	100
slp03	3158	0	0	0	0	100	100
slp04	3593	0	0	0	0	100	100
slp14	2857	0	0	0	0	100	100
slp16	3768	0	0	0	0	100	100
slp32	3041	0	1	1	0.03	99.97	100
slp37	3620	0	0	0	0	100	100
slp41	2831	50	30	80	1.06	99.4	99.54
slp45	3370	7	7	14	0.42	99.79	99.79
slp48	2981	11	2	13	0.44	99.93	99.63
slp59	3319	0	5	5	0.15	99.85	100
slp60	3271	7	0	7	0.21	100	99.79
slp61	3177	25	7	32	1.01	99.78	99.22
slp66	3093	50	60	110	0.82	99.67	99.51
slp67x	3095	0	36	36	1.16	98.84	100
Total # of subjects		18		Sensitivity %		99.80	
Total # of complexes		58241		Positive predictivity %		99.86	

standard deviation of estimation will increase linearly with an increase in the noise standard deviation. Therefore, it can be inferred that the performance of the PPF algorithm changes in a uniform fashion with an increase in noise standard deviation. In other words, for a considerable increase in noise standard deviation, a uniform performance is resulted from the PPF algorithm. In Figure 9, the parameterized exponential kernel functions are illustrated. According to this figure, each an exponential kernel function is specified by two parameters (μ, σ). After regulating the RBF-SVM network with the structure shown in Figure 6, the parameters of each kernel function of the SVM structure are obtained, shown in Table 7 (using MIMICII database according to Table 8 specifications).

In Figures 10 to 12, HR, SBP, DBP and MAP signals averaged for three typical subjects of the MIMIC II Database are illustrated. Fast fluctuations can be observed in these figures, which are significantly due to regulating mechanisms rather than measurement noises. To obtain more accurate results, these fluctua-

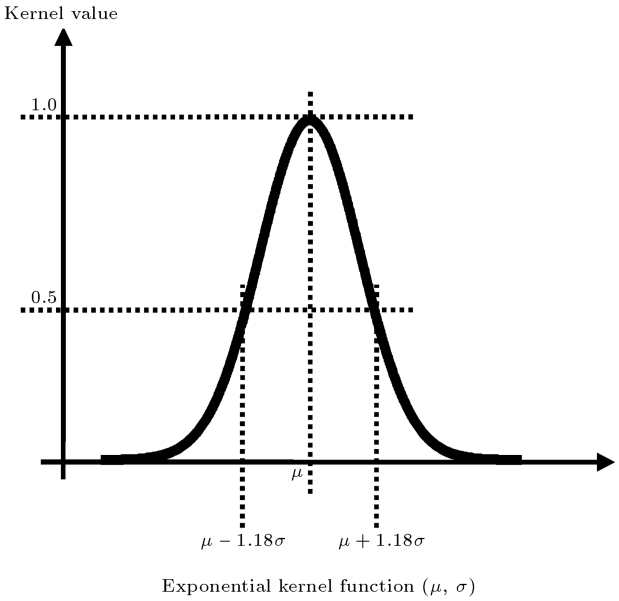

Figure 9. Parameterization of a generic exponential kernel function.

Table 7. Kernel function parameters of the RBF-SVM structure obtained after regulating.

Variable/ Parameter (Range)	Kernel#1 Parameters	Kernel#2 Parameters	Kernel#3 Parameters
HR [40-260] beats/min	(48.1514,21.2317)	(104.0193,23.8715)	(219.8417,45.2966)
SBP [80-280] mmHg	(74.9817,19.1744)	(101.3261,21.2519)	(227.0328,45.6217)
DBP [40-200] mmHg	(44.2567,14.6494)	(97.1583,21.4567)	(154.4349,19.6438)
Age [20-90] years	(233.5789,24.6312)	(251.2841,18.5647)	(279.8637,18.2849)
Gender male, female	(251.7119,23.3216)	—	—
Weight [40-220] kg	(37.5121,61.2353)	(94.5847,147.4595)	(171.0561,198.5255)

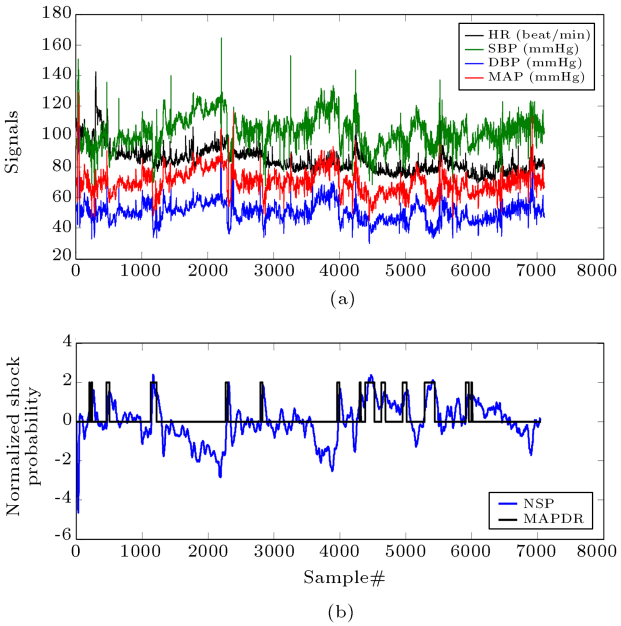

Figure 10. (a) HR, SBP, DBP and MAP trends averaged in one-minute intervals of s22466 of MIMIC II database obtained as outputs of BPMHT and ECGMHT algorithms. (b) Normalized shock probability obtained from SVM classifier and MAPDR signal.

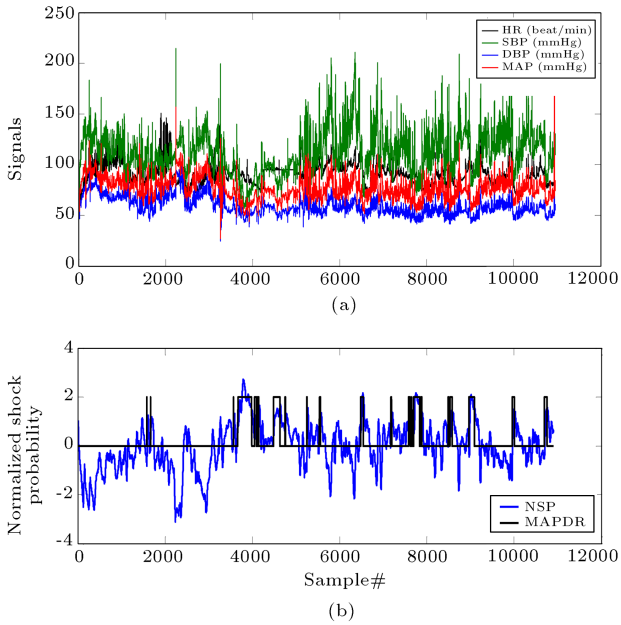

Figure 11. (a) HR, SBP, DBP and MAP trends averaged in one-minute intervals of s24799 of MIMIC II database obtained as outputs of BPMHT and ECGMHT algorithms. (b) Normalized shock probability obtained from RBF-SVM classifier and MAPDR signal.

tions should be decreased, while the signal mean value should not be destroyed by the reduction algorithm. Due to the difficulties in the recognition of the frequency contents of these fluctuations, common digital filters cannot be implemented for this purpose [37]. On the other hand, the reference signal should be known, so that adaptive filters can be used [27]. Therefore, an appropriate mean estimator is needed to weaken the fluctuations not similar to white noise. An averaged MAP signal with the corresponding PPF resulted smoothed signal for a typical subject is depicted in Figure 13. The magnified part of Figure 13 illustrates the operation of the PPF algorithm in the elimination of MAP fluctuations. Generally speaking, elimination of the MAP and HR fluctuations will lead to the higher stability and accuracy of the detection algorithms.

Names of records extracted from the Physionet database are presented in Table 8. From the parameters needed in the Hasdai et al. model, HR, SBP, DBP, age and gender are available. However, other parameters, such as treatment, MI location, Killip class, weight, and other miscellaneous factors are not

Table 8. Specifications of the under-study subjects obtained from MIMIC II Database. Due to the lack of sufficient clinical data, the parameter treatment, MI location and Killip Class are chosen as the zero risk scores equivalence.

	Parameter Assignment for CinC Challenge 2009 Database						Performance of the SVM-Based Classifier				
	Record # (Gender, Age)	# of Mean Sample	Treatment	MI Location	Killip Class	Miscellaneous Grade	Detection		Prediction		Error
							True	Eval.	True	Eval.	
AHE in Forecast Window, Treated with Pressors	S21775 (M-75)	22143	TPA	Other	I	10	AHE	AHE	AHE	AHE	NO
	S20658 (M-72)	24704	TPA	Other	I	10	AHE	AHE	AHE	AHE	NO
	S22466 (F-76)	8287	TPA	Other	I	13	AHE	AHE	AHE	AHE	NO
	S05336 (M-40)	4294	TPA	Other	I	10	AHE	AHE	AHE	AHE	NO
	S06349 (F-89)	17506	TPA	Other	I	13	AHE	AHE	AHE	AHE	NO
	S08718 (M-88)	10025	TPA	Other	I	10	AHE	AHE	AHE	AHE	NO
	S20794 (M-85)	5880	TPA	Other	I	10	AHE	CRT	AHE	CRT	YES
	S24799 (M-66)	4411	TPA	Other	I	10	AHE	AHE	AHE	AHE	NO
	S26318 (M-65)	7410	TPA	Other	I	10	AHE	N	AHE	N	YES
	S14204 (F-89)	14412	TPA	Other	I	13	AHE	CRT	AHE	AHE	NO
	S25699 (M-35)	15717	TPA	Other	I	10	AHE	AHE	AHE	AHE	NO
	S07125 (M-53)	6487	TPA	Other	I	10	AHE	AHE	AHE	AHE	NO
	S19208 (F-78)	18804	TPA	Other	I	13	AHE	CRT	AHE	CRT	YES
	S12821 (F-77)	16042	TPA	Other	I	13	AHE	AHE	AHE	AHE	NO
	S06637 (M-78)	2898	TPA	Other	I	10	AHE	AHE	AHE	AHE	NO
AHE in Forecast Window, not Treated with Pressors	S02395 (F-80)	5355	TPA	Other	I	13	AHE	CRT	AHE	CRT	YES
	S08779 (M-58)	6750	TPA	Other	I	10	AHE	AHE	AHE	AHE	NO
	S23641 (M-90)	8639	TPA	Other	I	10	AHE	AHE	AHE	AHE	NO
	S24924 (F-79)	5453	TPA	Other	I	13	AHE	AHE	AHE	AHE	YES
	S00439 (F-82)	11616	TPA	Other	I	13	AHE	CRT	AHE	N	NO
	S23015 (M-68)	4267	TPA	Other	I	10	AHE	AHE	AHE	AHE	NO
	S19603 (F-75)	2853	TPA	Other	I	13	AHE	AHE	AHE	AHE	NO
	S02172 (M-32)	4471	TPA	Other	I	10	AHE	AHE	AHE	AHE	NO
	S26105 (M-47)	17078	TPA	Other	I	13	AHE	AHE	AHE	AHE	NO
	S23599 (F-66)	11756	TPA	Other	I	13	AHE	AHE	AHE	AHE	NO
	S21817 (F-73)	8280	TPA	Other	I	13	AHE	AHE	AHE	AHE	NO
	S24984 (M-56)	35896	TPA	Other	I	10	AHE	AHE	AHE	AHE	NO
	S25602 (F-77)	4090	TPA	Other	I	13	AHE	N	AHE	N	YES
	S23591 (M-85)	6586	TPA	Other	I	10	AHE	AHE	AHE	AHE	NO
	S15687 (F-90)	8340	TPA	Other	I	13	AHE	AHE	AHE	AHE	NO
Records not Containing AHEs	S17765 (M-51)	2370	TPA	Other	I	10	N	N	N	N	NO
	S04860 (F-57)	5394	TPA	Other	I	13	N	N	N	N	NO
	S26097 (F-42)	11755	TPA	Other	I	13	N	N	N	N	NO
	S00318 (M-58)	2953	TPA	Other	I	10	N	N	N	N	NO
	S14495 (M-59)	1746	TPA	Other	I	10	N	N	N	N	NO
	S22888 (M-48)	1093	TPA	Other	I	10	N	N	N	N	NO
	S26296 (M-47)	3699	TPA	Other	I	10	N	N	N	N	NO
	S06180 (F-45)	3252	TPA	Other	I	13	N	N	N	N	NO
	S07468 (F-71)	6837	TPA	Other	I	13	N	N	N	N	NO
	S24004 (M-66)	2581	TPA	Other	I	10	N	N	N	N	NO
	S03133 (M-46)	1706	TPA	Other	I	10	N	N	N	N	NO
	S02280 (M-58)	2127	TPA	Other	I	10	N	N	N	N	NO
	S09672 (F-46)	2503	TPA	Other	I	13	N	N	N	CRT	NO
	S19418 (F-39)	3037	TPA	Other	I	13	N	N	N	N	NO
	S15465 (M-67)	1590	TPA	Other	I	13	N	N	N	N	NO
AHE, but not in Forecast window	S05786 (M-54)	8795	TPA	Other	I	13	CRT	CRT	CRT	CRT	NO
	S25222 (F-60)	1749	TPA	Other	I	13	CRT	CRT	CRT	CRT	NO
	S02561 (F-81)	18645	TPA	Other	I	13	CRT	CRT	CRT	CRT	NO
	S24923 (F-82)	23625	TPA	Other	I	13	CRT	CRT	CRT	CRT	NO
	S16019 (F-90)	2861	TPA	Other	I	13	CRT	CRT	CRT	CRT	NO
	S04286 (M-61)	13979	TPA	Other	I	10	CRT	CRT	CRT	CRT	NO
	S17069 (F-61)	7047	TPA	Other	I	13	CRT	AHE	CRT	AHE	NO
	S07860 (F-36)	7047	TPA	Other	I	13	CRT	AHE	CRT	AHE	NO
	S23020 (F-84)	15878	TPA	Other	I	13	CRT	CRT	CRT	CRT	NO
	S24431 (M-22)	11982	TPA	Other	I	10	CRT	N	CRT	N	YES
	S22657 (M-88)	33007	TPA	Other	I	10	CRT	N	CRT	N	YES
	S09341 (F-62)	33132	TPA	Other	I	13	CRT	CRT	CRT	CRT	NO
	S05126 (F-69)	13055	TPA	Other	I	13	CRT	CRT	CRT	CRT	NO
	S10611 (M-78)	5652	TPA	Other	I	10	CRT	CRT	CRT	CRT	NO
	S05289 (M-76)	11483	TPA	Other	I	10	CRT	CRT	CRT	CRT	NO
Total Number	**581,030**						**Se = 92%**		**$P+ = 93\%$**		

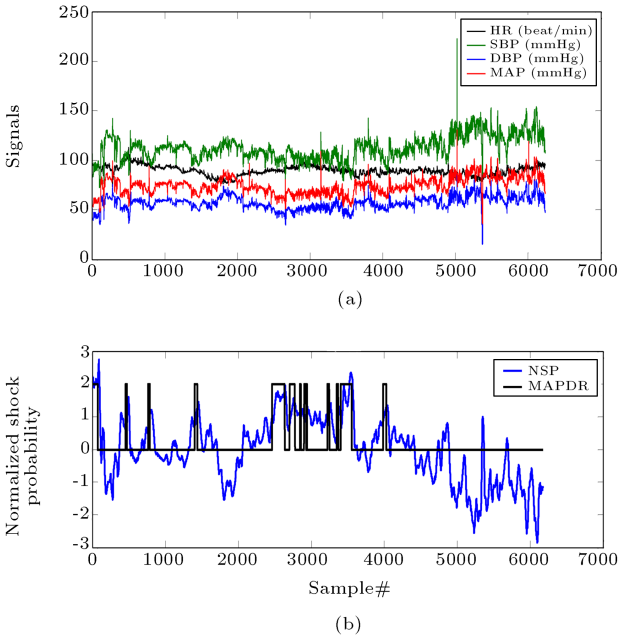

Figure 12. (a) HR, SBP, DBP and MAP trends averaged in one-minute intervals of s25699 of MIMIC II database obtained as outputs of BPMHT and ECGMHT algorithms. (b) Normalized shock probability obtained from SVM classifier and MAPDR signal.

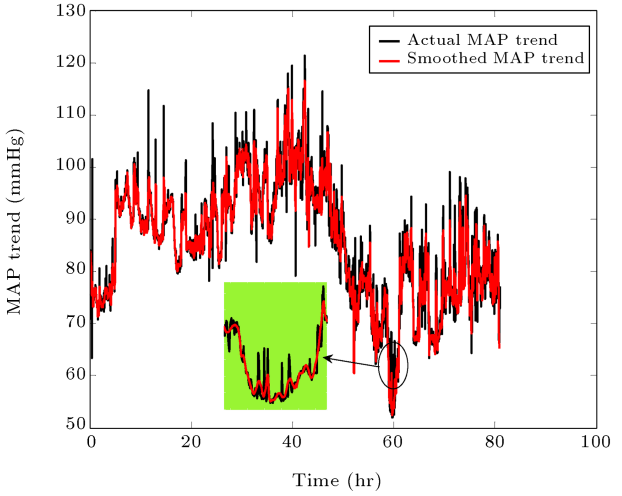

Figure 13. Averaged MAP trend and the corresponding PPF smoothed version for a typical subject. The magnified part shows the capability of the algorithm in the elimination of fast fluctuations.

known and, therefore, are set equal to average values according to Table 8.

The probability of cardiogenic shock occurrence and scaled MAPDR graphs are represented in Figure 14. The red graphs in this figure have a baseline, which is a sign of no MAPDR; however, abrupt increase to the maximum value is an indicator of MAPDR. As can be seen in Figure 14, a high peak between 29 hrs and 30 hrs in the probability of shock occurrence

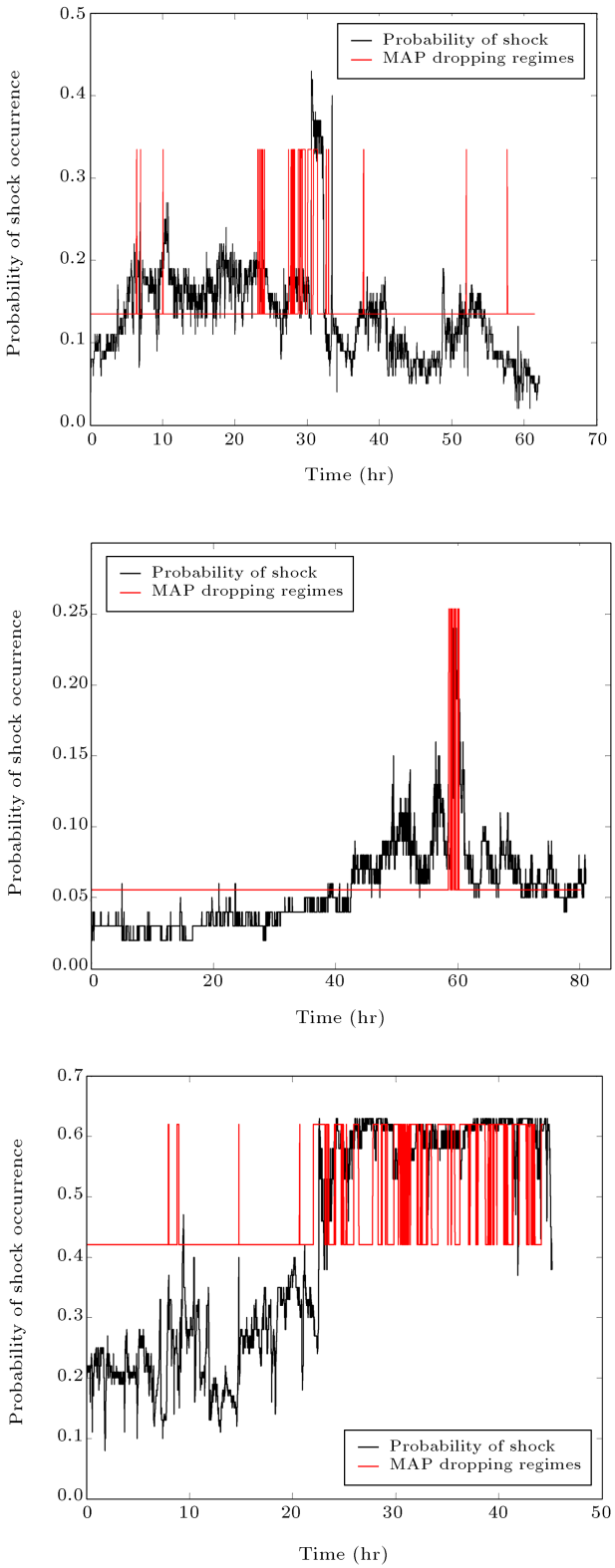

Figure 14. Magnifications in the MAPDR occurrence and cardiogenic shock probability trends in 3 generic AHE records of MIMICII database. In these graphs, fast fluctuations occur with no high duration. However, fast fluctuations with high endurance as well as a peak in the probability occurrence trend are observed after T_0 (beginning of shock) time.

graph is preceded by continuous fluctuations in the corresponding red graph. The results of this study show that all high peaks with 3 to 4 minutes duration in the probability of shock occurrence graph are preceded by peaks in the MAPDR signal with a duration of 20 minutes or more (see Figures 10 to 12). Therefore, as a result of this study, MAPDRs can be used as specific markers for the prediction of cardiogenic shock. It should be noted that there may exist some continuous fluctuations in MAPDR with no corresponding high peaks in the probability of shock occurrence graph. This can be due to the short duration of such fluctuations. In summary, these fluctuations should have duration of 20 minutes or more, so that high peaks with duration of 3 or more minutes occur in the probability of shock occurrence diagram.

CONCLUSION

In this study, in order to consider the mutual influence of parameters on the evaluation of shock probability, a RBF based support vector machine classifier was tuned using features extracted from the Hasdai et al. risk scoring model as input, with appropriate exponential kernel functions for each parameter. Using this network, it would be possible to incorporate the possible mutual influences between risk parameters, such as Heart Rate (HR), Systolic Blood Pressure (SBP), Diastolic Blood Pressure (DBP), age, gender, weight and some miscellaneous factors, to the calculation of shock occurrence probability.

The MHT algorithm was introduced for the detection of QRS complexes and blood pressure pulses on the basis of some mathematical operations on the Hilbert transform of the ECGMHT and ABP signals. It was then customized with two versions of ECGMHT and BPMHT to be applied to ECG signals and ABP waveforms, respectively. After applying this algorithm to the MIT-BIH Database, values of 99.80% and 99.85% were obtained for sensitivity and positive prediction, which are remarkably acceptable in the field of wave detection. In the next step, the PPF algorithm was developed for the elimination of fast fluctuations with unknown statistical specifications. The ECGMHT and BPMHT algorithms were then applied to 15 subjects of the MIMIC II Database and the resulted averaged MAP, SBP, DBP and HR trends were next smoothed using the FFT algorithm. Afterwards, a new measure entitled MAPDR was proposed as an indicator of descending behavior in the MAP trend when AHE occurs, and was calculated using the resulted PPF signals.

In the next step, a RBF-SVM classifier was tuned using features obtained from the cardiogenic shock risk scoring model developed by Hasdai et al. (2000), which classifies MAP regimes into three categories: survival, critical and Acute Hypotensive Episode (AHE). Then, the regulated RBF-SVM classifier was applied to 60 records of the CinC Challenge 2009 and the values of Se = 92% and $P+$ = 93% were obtained for sensitivity and positive predictivity, respectively. As some results of this study, the proposed classification method recognized truly 15 subjects out of 15 normal (without shock episodes) subjects of the MIMICII database as belonging to the "survival class", while the algorithm could classify 24 subjects as "AHE", 3 subjects as "critical class" and 3 subjects as in a "survival" situation out of 30 shock containing records of the MIMICII database.

LIST OF ACRONYMS

ICU	Intensive Care Unit
AHE	Acute Hypotensive Episode
MHT	Modified Hilbert Transform
ABP	Arterial Blood Pressure
SBP	Systolic Blood Pressure
DBP	Diastolic Blood Pressure
MAP	Mean Arterial Pressure
PPF	Piecewise Polynomial Fitting
BLUE	the Best Linear Unbiased Estimation
MAPDR	Mean Arterial Pressure Dropping Regime
HR	Heart Rate
MIMIC	name of physionet database
PCA	Principal Component Analysis
RBF	Radial Basis Function
SVM	Support Vector Machine
BP	Blood Pressure
BPMHT	name of the blood pressure pulse detector
ECGMHT	name of the QRS detector
NSP	Normalized Shock Probability
MI	Myocardial Infarction
PVC	Premature Ventricular Contraction
PAC	Premature Atrial Contraction
FP	False Positive
FN	False Negative
TP	True Positive
Se	sensitivity
$P+$	positive predictivity
DI	Dropping Index

REFERENCES

1. Guyton, A.C., *Text Book of Physiology*, **I**, Philadelphia, W.B. Saunders, Ed. (1996).
2. *Harrison's Principles of Internal Medicine*, 17th Ed., the McGraw-Hill Companies (2007).
3. Irwin, R.S. and Rippe, J.M., *Irwin and Rippe's Intensive Care Medicine*, Lippincott Williams & Wilkins, 5th Ed. (2003).
4. Marino, P., *The ICU Book, Lippincott Williams & Wilkins*, 2nd Ed. (1978).

5. Cowley, A.W., Liard, J.F. and Guyton, A.C. "Role of the baroreceptor reflex in daily control of arterial blood pressure and other variables in dogs", *Circ. Res.*, **32**, pp. 564-576 (1973).
6. Hasdai, D., Califf, R.M., Thompson, T.D., Hochman, J.S., Ohman, E.M., Pfisterer, M., Bates, E.R., Vahanian, A., Armstrong, P.W., Criger, D.A., Topol, E.J. and Holmes, D.R. "Predictors of cardiogenic shock after thrombolytic therapy for acute myocardial infarction", *J. Am. Coll. Cardiol.*, **35**, pp. 136-143 (2000).
7. Picard, M.H., Davidoff, R., Sleeper, L.A., Mendes, L.A., Thompson, C.R., Dzavik, V., Steingart, R., Gin, K., White, H.D. and Hochman, J.S. "Echocardiographic predictors of survival and response to early revascularization in cardiogenic shock and for the SHOCK trial", *Circulation*, **107**, pp. 279-284 (2003).
8. Morris, R.W., Watterson, L.M., Westhorpe, R.N. and Webb, R.K. "Crisis management during anesthesia: Hypotension", *Qual. Saf. Health Care*, **14**, e11 (2005).
9. Solem, K., Nilsson, A. and Sornmo, L. "Detection of hypotension during hemodialysis using the ECG", *Computers in Cardiology*, **31**, pp. 717-720 (2004).
10. Halkin, A., Singh, M., Nikolsky, E., Grines, C.L., Tcheng, J.E., Garcia, E., Cox, D.A., Turco, M., Stuckey, T.D., Na, Y., Lansky, A.J., Gersh, B.J., O'Neill, W.W., Mehran, R. and Stone, G.W. "Prediction of mortality after primary percutaneous coronary intervention for acute myocardial infarction, the CADILLAC risk score", *J. Am. Coll. Cardiol.*, **45**, pp. 1397-1405 (2005).
11. Zhang, M., Li, J., Cai, Y.M., Ma, H., Xiao, J.M., Liu, J., Zhao, L., Guo, T. and Han, M.H. "A risk-predictive score for cardiogenic shock after acute myocardial infarction in Chinese patients", *Clin. Cardiol.*, **30**, pp. 171-176 (2007).
12. Moody, G.B. and Lehman, L.H. "Predicting acute hypotensive episodes: The 10th annual physioNet/computers in cardiology challenge", *The Proceedings of Computers in Cardiology Challenge 2009*, Lake-city, Utah (2009).
13. Chen, X., Xu, D., Zhang, G. and Mukkamala, R. "Forecasting acute hypotensive episodes in intensive care patients based on a peripheral arterial blood pressure waveform", *The Proceedings of Computers in Cardiology Challenge 2009*, Lake-city, Utah (2009).
14. Henriques, J.H. and Rocha, T.R. "Prediction of acute hypotensive episodes using neural network multimodels", *The Proceedings of Computers in Cardiology Challenge 2009*, Lake-city, Utah (2009).
15. Langley, P., King, S.T., Zheng, D., Bowers, E.J., Wang, K., Allen, J. and Murray, A. "Predicting acute hypotensive episodes from mean arterial pressure", *The Proceedings of Computers in Cardiology Challenge 2009*, Lake-city, Utah (2009).
16. Mneimneh, M.A. and Povinelli, R.J. "A rule-based approach for the prediction of acute hypotensive episodes", *The Proceedings of Computers in Cardiology Challenge 2009*, Lake-city, Utah (2009).
17. Chiarugi, F., Karatzanis, I., Sakkalis, V., Tsamardinos, I., Dermitzaki, T.H., Foukarakis, M. and Vrouchos, G. "Predicting the occurrence of acute hypotensive episodes: The physioNet challenge", *The Proceedings of Computers in Cardiology Challenge 2009*, Lake-city, Utah (2009).
18. Fournier, P.A. and Roy, J.F. "Acute hypotension episode prediction using information divergence for feature selection, and non-parametric methods for classification", *The Proceedings of Computers in Cardiology Challenge 2009*, Lake-city, Utah (2009).
19. Hayn, D., Jammerbund, B., Kollmann, A. and Schreier, G. "A biosignal analysis system applied for developing an algorithm predicting critical situations of high risk cardiac patients by hemodynamic monitoring", *The Proceedings of Computers in Cardiology Challenge 2009*, Lake-city, Utah (2009).
20. Jin, K. and Stockbridge, N., *Smoothing and Discriminating MAP Data. The Proceedings of Computers in Cardiology Challenge 2009*, Lake-city, Utah (2009).
21. Jousset, F., Lemay, M. and Vesin, J.M. "Computers in cardiology/physioNet challenge 2009: Predicting acute hypotensive episodes", *The Proceedings of Computers in Cardiology Challenge 2009*, Lake-city, Utah (2009).
22. Ho, T.C.T. and Chen, X. "Utilizing histogram to identify patients using pressors for acute hypotension", *The Proceedings of Computers in Cardiology Challenge 2009*, Lake-city, Utah (2009).
23. Ghaffari, A. and Homaeinezhad, M.R. "Fading parameters of sodium, potassium and leakage ionic channels the Best Linear Unbiased sequentially Estimation (BLUE) via voltage clamp technique noisy measurement", *16th Annual (International) Conference on Mechanical Engineering-ISME*, Shahid Bahonar University of Kerman, Iran (14-16 May 2008).
24. Benitez, D., Gaydecki, P.A., Zaidi, A. and Fitzpatrick, A.P. "The use of the Hilbert transform in ECG signal analysis", *Computers in Biology and Medicine*, **31**, pp. 399-406 (2001).
25. Arzeno, N.M., Deng, Z. and Poon, C.S. "Analysis of first-derivative based QRS detection algorithms", *IEEE Transactions on Biomedical Engineering*, **55**(2), pp. 478-484 (2008).
26. Söderström, T. and Stoica, P., *System Identification*, Hemel Hempstead, UK, Prentice-Hall International (1989).
27. Kay, S.M., *Fundamentals of Statistical Signal Processing: Estimation Theory*, Prentice-Hall Inc. (1979).
28. Bishop, C.M., *Pattern Recognition and Machine Learning*, Springer Publishing (2006).
29. Hasdai, D., Berger, P.B., Battler, A. and Holmes, D.R., *Cardiogenic Shock, Diagnosis and Treatment*, Hummana Press (2008).

30. Physionet Signal Archieves, http://www. physionet.org/physiobank/database/mitdb/ and http: // www. physionet. org/physiobank/database/slpdb/.

31. Ghaffari, A., Homaeinezhad, M.R., Akraminia, M., Atarod, M. and Davaeeha, M. "A robust wavelet-based multi-lead electrocardiogram delineation algorithm", *Medical Engineering & Physics*, in press (2009).

32. Martinez, J.P., Almeida, R., Olmos, S., Rocha, A.P. and Laguna, P. "A wavelet-based ECG delineator: Evaluation on standard databases", *IEEE Transactions on Biomedical Engineering*, **51**(4), pp. 570-581 (2004).

33. Li, C., Zheng, C. and Tai, C. "Detection of ECG characteristic points using wavelet transforms", *IEEE Transactions on Biomedical Engineering*, **42**, pp. 21-28 (1995).

34. Hamilton, P.S. and Tompkins, W. "Quantitative investigation of QRS detection rules using the MIT/BIH arrhythmia database", *IEEE Transactions on Biomedical Engineering*, **33**, pp. 1157-1165 (1986).

35. Pan, J. and Tompkins, W.J. "A real-time QRS detection algorithm", *IEEE Transactions on Biomedical Engineering*, **32**, pp. 230-236 (1985).

36. Moody, G.B. and Mark, R.G. "Development and evaluation of a 2-lead ECG analysis program", *Proceeding of Computers in Cardiology*, pp. 39-44 (1982).

37. Rangayyan, R.M., *Biomedical Signal Analysis*, IEEE Press, John Wiley and Sons (2002).

BIOGRAPHIES

Ali Ghaffari was born in Neyshabour in 1945. He received BS, MS and PhD degrees all in Mechanical Engineering from Sharif University of Technology, Georgia Institute of Technology and University of California at Berkeley in 1969, 1973 and 1976, respectively. Since, 1979, he has been with the Department of Mechanical Engineering of K. N. Toosi University of Technology. Professor Ghaffari's research is mainly focused on Dynamic Systems and Control, including: Analysis of Stochastic Phenomena, Dynamics and Control of Nonlinear Systems, Application of Fuzzy Set Theory and Artificial Neural Networks to Mechanical Systems, and Biomedical Signal Processing, specifically ECG.

Mohammad Reza Homaeinezhad was born in Shiraz, Iran, in 1980. He received his BS and MS degrees (with best honors) both in Mechanical Engineering and Dynamic Systems and Control from K. N. Toosi University of Technology, Tehran, Iran, where he is currently a PhD candidate of Mechanical Engineering. His research interests include: Nonlinear Dynamics and Control, Statistical Signal Analysis and Parameter Estimation, Automatic Decision Making (detection & modulation) Theory and Biomedical Waveforms (BP, ECG & PCG) Processing.

Mahdi Akraminia was born in Tehran, Iran, in 1985. He received his BS degree in Mechanical Engineering, Dynamic Systems and Control from K. N. Toosi University of Technology, Tehran, Iran, in 2007 where he is now pursuing his MS degree.

Mohammad Atarod Pilambaraei was born in Talesh, Guilan, Iran, in 1984. He graduated from K. N. Toosi University of Technology in 2009 with an MS degree in Mechanical Engineering. He is currently doing his PhD in Biomedical Engineering at the University of Calgary, Alberta, Canada. His research is mainly focused on: Biomechanics, including Biomechanics of the Cardiovascular System and Knee Joints.

Reza Rahmani was born in Tehran in 1963. He received his Medical Doctoral degree, board certification and higher board professional certification all in cardiology from Tehran University of Medical Sciences (TUMS) in 1994, 2002 and 2005, respectively. Since 2007, he has been with the School of Medicine of the TUMS as a Cardiology Assistant Professor. Also, he is currently a member of the Catheter and Angiography Laboratory of Imam Khomeini Hospital, Tehran, Iran.